^{31}P magnetization transfer measurements of $P_i \rightarrow$ATP flux in exercising human muscle

Alison Sleigh,[1,2] David B. Savage,[3] Guy B. Williams,[1] David Porter,[4] T. Adrian Carpenter,[1] Kevin M. Brindle,[5,6] and Graham J. Kemp[7,8]

[1]*Wolfson Brain Imaging Centre, University of Cambridge School of Clinical Medicine, Cambridge Biomedical Campus, United Kingdom;* [2]*National Institute for Health Research/Wellcome Trust Clinical Research Facility at Cambridge University Hospitals NHS Foundation Trust, Cambridge Biomedical Campus, United Kingdom;* [3]*University of Cambridge Metabolic Research Laboratories, Wellcome Trust-Medical Research Council Institute of Metabolic Science, Cambridge Biomedical Campus, United Kingdom;* [4]*Fraunhofer MEVIS, Institute for Medical Image Computing, Bremen, Germany;* [5]*Department of Biochemistry, University of Cambridge, United Kingdom;* [6]*Cancer Research UK Cambridge Institute, Li Ka Shing Centre, University of Cambridge, Cambridge Biomedical Campus, United Kingdom;* [7]*Magnetic Resonance and Image Analysis Research Centre, University of Liverpool, United Kingdom; and* [8]*Department of Musculoskeletal Biology and MRC - Arthritis Research UK Centre for Integrated research into Musculoskeletal Ageing, Institute of Ageing and Chronic Disease, University of Liverpool, United Kingdom*

Sleigh A, Savage DB, Williams GB, Porter D, Carpenter TA, Brindle KM, Kemp GJ. ^{31}P magnetization transfer measurements of $P_i \rightarrow$ATP flux in exercising human muscle. *J Appl Physiol* 120: 649–656, 2016. First published January 7, 2016; doi:10.1152/japplphysiol.00871.2015.— Fundamental criticisms have been made over the use of ^{31}P magnetic resonance spectroscopy (MRS) magnetization transfer estimates of inorganic phosphate (P_i)→ATP flux ($V_{P_i\text{-}ATP}$) in human resting skeletal muscle for assessing mitochondrial function. Although the discrepancy in the magnitude of $V_{P_i\text{-}ATP}$ is now acknowledged, little is known about its metabolic determinants. Here we use a novel protocol to measure $V_{P_i\text{-}ATP}$ in human exercising muscle for the first time. Steady-state $V_{P_i\text{-}ATP}$ was measured at rest and over a range of exercise intensities and compared with suprabasal oxidative ATP synthesis rates estimated from the initial rates of postexercise phosphocreatine resynthesis (V_{ATP}). We define a surplus P_i→ATP flux as the difference between $V_{P_i\text{-}ATP}$ and V_{ATP}. The coupled reactions catalyzed by the glycolytic enzymes GAPDH and phosphoglycerate kinase (PGK) have been shown to catalyze measurable exchange between ATP and P_i in some systems and have been suggested to be responsible for this surplus flux. Surplus $V_{P_i\text{-}ATP}$ did not change between rest and exercise, even though the concentrations of P_i and ADP, which are substrates for GAPDH and PGK, respectively, increased as expected. However, involvement of these enzymes is suggested by correlations between absolute and surplus P_i→ATP flux, both at rest and during exercise, and the intensity of the phosphomonoester peak in the ^{31}P NMR spectrum. This peak includes contributions from sugar phosphates in the glycolytic pathway, and changes in its intensity may indicate changes in downstream glycolytic intermediates, including 3-phosphoglycerate, which has been shown to influence the exchange between ATP and P_i catalyzed by GAPDH and PGK.

^{31}P magnetization transfer; saturation transfer; $P_i \leftrightarrow$ATP exchange; exercising muscle

MAGNETIZATION TRANSFER MEASUREMENTS using ^{31}P magnetic resonance spectroscopy (MRS) of flux between inorganic phosphorus (P_i) and ATP (P_i→ATP), here called saturation transfer (ST), have been widely implemented for the putative assessment of mitochondrial function in skeletal muscle. In 2008, Kemp (13) drew attention to the striking fact that in resting muscle ST is an order of magnitude larger than the net rate of oxidative ATP synthesis that it was claimed to measure, a discrepancy too large to be compensated by the use of relative data presentations such as test/control or post/pre ratios. This and the separate point that a resting flux has no straightforward relationship to metabolic capacity (13, 16) have stimulated much recent debate over the interpretation of this measurement (2, 3, 11, 16, 27, 29, 35).

This discrepancy between ST and known or inferred rates of oxidative ATP synthesis (which we call here the "surplus" ST rate) in skeletal muscle is usually attributed to a rapid, near-equilibrium $P_i \leftrightarrow$ATP exchange catalyzed by the glycolytic enzymes GAPDH (EC 1.2.1.12) and phosphoglycerate kinase (PGK; EC 2.7.2.3). Some early ST measurements of P_i→ATP flux in *Saccharomyces cerevisiae* (5, 6, 9) provided evidence for a GAPDH/PGK-mediated exchange contribution. In addition, an in vitro study (8) showed that this GAPDH/PGK couple could, with simulated levels of enzymes and substrates, catalyze sufficient P_i-ATP exchange to explain data obtained in glucose-perfused rat heart. This was subsequently confirmed by Kingsley-Hickman et al. (20) in intact perfused rat myocardium, when they manipulated glycolysis over a range of oxygen consumption rates. GAPDH and PGK activities are similar in human and rat heart and in rat skeletal and human intercostal muscle (31, 32). Although GAPDH activity is lower in human skeletal muscle compared with rat skeletal muscle (106 ± 28 vs. 294 ± 36 U/g tissue), it is still similar or greater than that of rat heart (31, 32).

Another potential explanation for a surplus P_i→ATP flux relates to a mitochondrial P_i-ATP exchange. LaNoue et al. (21) used ^{33}P-radiolabeled tracers in isolated rat liver and heart mitochondria to demonstrate a significant ATP→P_i flux (i.e., in the reverse direction of ATP synthesis), and thus unidirectional P_i→ATP rates in excess of the net ATP synthesis rate. In the transition from zero to maximal net ATP synthesis (in moving from state 4 to state 3 respiration) the P_i→ATP flux doubled, whereas the reverse ATP→P_i flux decreased by >90%. Sheldon and Brindle et al. (30) also provided evidence for a

Address for reprint requests and other correspondence: A. Sleigh, Wolfson Brain Imaging Centre, University of Cambridge, Box 65 Addenbrooke's Hospital, Cambridge Biomedical Campus, Cambridge, CB2 0QQ, U.K. (e-mail: as626@wbic.cam.ac.uk).

mitochondrial P_i-ATP exchange in vivo using ST measurements in yeast when they removed the glycolytic exchange catalyzed by GAPDH and PGK by lowering PGK expression using an attenuated promoter. Subtraction of the net glycolytic P_i→ATP flux, estimated from measurements of glucose consumption, showed that overexpression of the adenosine nucleotide translocase (ANT) significantly increased the P_i→ATP flux determined using ST measurements.

Other explanations proposed for the anomalously large P_i-ATP flux, such as rapidly exchanging small pools of metabolites (2), remain speculative. For skeletal muscle the literature generally has been interpreted as favoring a glycolytic P_i-ATP exchange mediated by the GAPDH/PGK couple (16, 27, 35), although it has been speculated (3, 11, 30) that in resting muscle with its low respiration rates, mitochondrial-associated P_i-ATP exchange may become more prominent (21).

To investigate the determinants of this flux in vivo, we set out to define the effects of varying oxidative ATP synthesis rates on ST measurements in human skeletal muscle, which has been the main organ of interest in recent ST studies. There have been few studies of ST over a range of respiration rates: in stimulated rat hindlimb muscle (7), in lamb myocardium in vivo (26) and perfused rat myocardium (20), and in rat brain under varying levels of anesthesia (10). The rat hindlimb study (7) has been incorrectly cited (12, 22, 37) as supporting the validity of the resting ST as a measure of oxidative ATP synthesis. That study showed only that the P_i→ATP flux in the stimulated muscle was not very different from the rates of net oxidative ATP synthesis observed in other studies that used similar experimental preparations and concluded that a glycolytic exchange contribution could not be ruled out, particularly in resting muscle. The lamb and rat myocardium studies (20, 26) found that the surplus P_i→ATP flux remained approximately constant, or decreased, with increasing oxidative ATP synthesis rate. A retrospective comparison of the rat hindlimb results (7) with a range of published non-ST data resulted in similar findings (13). In the brain study (10), oxygen consumption was not measured. To study this relationship directly we designed a protocol to measure the steady-state rates of P_i→ATP flux over a range of exercise intensities in human skeletal muscle and compared these with immediate postexercise rates of phosphocreatine (PCr) resynthesis, which are a measure of the suprabasal end-exercise mitochondrial oxidative ATP synthesis rate (15). We hypothesized that the surplus P_i→ATP flux was a result of the exchange catalyzed by GAPDH and PGK and that this would remain unchanged, or decrease, with increasing oxidative ATP synthesis rate.

METHODS

Participants. Each participant provided written informed consent and all studies were conducted in accordance with the Declaration of Helsinki. Ethical approval was granted by the UK National Research Ethics Service. Eleven healthy adult volunteers (7 men, 4 women) were recruited (age, 29.4 ± 2.8 yr; body mass index, 22.8 ± 0.9 kg/m^2; means $\pm$ SE). Exclusion criteria included standard magnet contraindications, diabetes mellitus, cardiovascular disease, inability to understand protocol instructions, smoking, and taking medication or supplements known to affect energy metabolism.

Protocol. Participants were recruited into *group A* or *group B*, except one volunteer who entered both groups. *Group A* consisted of nine volunteers who undertook a single ^{31}P MRS scan with a work-load predetermined using a fraction of their previously measured maximum voluntary contraction force. To test the feasibility of this exercise protocol in a variety of participants and over a range of ATP turnover rates, this fraction was varied among the volunteers. The three participants in *group B* undertook 4 ^{31}P MRS scans on different days; the workload varied between visits, yielding sufficient PCr depletion (for measurement of PCr resynthesis) at low workloads while maintaining the exercise tolerability and minimal acidification at higher workloads.

On a prescanning visit, each volunteer's maximum voluntary contraction force was measured using a leg dynamometer (set to the same initial angle of exercise as in the magnetic resonance scanner), and all volunteers were shown an instruction video and given the opportunity to practice to ensure they were comfortable with the full in-scanner exercise protocol.

^{31}P *MRS.* Studies used a Siemens MAGNETOM 3T Verio (Erlangen, Germany) scanner, and each ^{31}P MRS scan consisted of resting and exercising ST measurements, and assessment of postexercise PCr recovery kinetics (Fig. 1). The volunteers were positioned supine and a 6-cm-diameter surface coil (RAPID Biomedical, Rimpar, Germany) was attached at the right rectus femoris muscle (which was a location that gave the maximal PCr depletion/workload ratio). Precise coil relocation for participants in *group B* was obtained by using approximate anatomical distances and then accurately by three-dimensional fasciae landmarks. A magnetic resonance-compatible weight was attached to the right ankle (33) to provide the predetermined workload.

Resting ST measurement. P_i magnetization was measured in the presence of selective saturation of the γ-ATP resonance (SAT) and compared with a control in which the irradiation frequency was placed symmetrical to the P_i peak (CONT) using a 1.32-ms BIR-4 adiabatic excitation (34) placed symmetrically between P_i and γ-ATP [repetition time (TR) = 24 s, receiver bandwidth (rBW) = 2,500 Hz, and number of acquisitions (NA) = 48 for each SAT/CONT]. The T_1 of P_i with saturation of the γ-ATP resonance (T_1') was measured using an inversion recovery (IR) pulse sequence [7 TIs between 9 and 10,000 ms, effective TR (TR_{eff}) = 6 s, NA = 12-20; TI was defined as the time between the inversion and subsequent excitation pulse, and TR_{eff} was defined as the time between the excitation and subsequent inversion pulse]. IR data were acquired in blocks that had the same TI, and the first spectrum of each group was eliminated. A fully relaxed spectrum was used to determine metabolite concentrations (NA = 12).

Exercising ST measurement. Figure 1 outlines the exercising ST protocol. Knee extensions were performed (0.5 Hz) and spectra (TR = 2 s) acquired to ensure steady state was reached before ST acquisition. A soft target was attached to the apex of the scanner bore to prevent participant hyperextension, inhibit waning, and aid in maintaining a steady state. For ST measurements, triggered headphone instructions gave warning and then instructed participants to be still during the excitation and subsequent acquisition; any noncompliance resulted in exclusion of that spectrum. Two minutes of exercise preceded the first useable SAT spectrum and the participants were considered not to be in steady-state exercise if their average [PCr] at time = 80 s differed by >2 standard deviations of the end of exercise [PCr] (Fig. 1). To avoid significant acidification and to increase tolerability of the protocol, the exercise was split into two bouts (shaded regions in Fig. 1). Due to the potential for lengthening of the P_i T_1 upon exercise (24), exercising ST parameters were similar to those of resting ST but with TR = 34 s, NA = 8 for each SAT/CONT; 5 TIs, NA = 6–15 for the T_1 measurement, and a TR of 44 s and NA = 4 for the metabolite spectra.

Postexercise PCr recovery kinetics. Ten spectra (TR 2 s) were obtained, which ensured that a steady-state magnetization had been reached (Fig. 1) before cessation of exercise and acquisition of spectra of the recovery kinetics (TR = 2 s, NA = 150). The PCr recovery rate constant, k_{PCr}, was found using a two-parameter monoexponential fit,
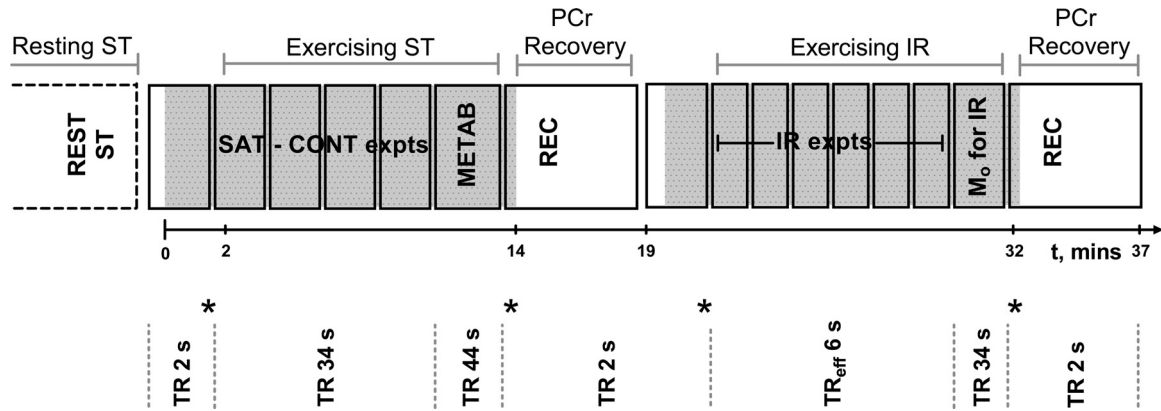
Fig. 1. Schematic representation of the ^{31}P magnetic resonance spectroscopy (MRS) exercise protocol. Solid lines symbolize sequence blocks, gray shaded regions correspond to when exercise occurred. Time from onset of exercise is illustrated by the timeline. In the first exercise section, once exercising steady-state conditions were met, spectra were obtained with saturation of the γ-ATP resonance and then control saturation placed equidistant to the inorganic phosphate (P$_i$) resonance (SAT-CONT expts). Spectra were also obtained with a long repetition time (TR) of 44 s for calculation of metabolite concentrations (METAB). Following exercise cessation a phosphocreatine (PCr) recovery measurement (REC) was used to assess the immediate end-of-exercise oxidative ATP synthesis rate. Within the second exercise, once in steady state, the inversion recovery data were acquired with varying times between the inversion and subsequent excitation pulse (TIs) (IR expts) with an effective TR of 6 s, and a measure of M$_o$ was also obtained. The four stars represent comparison sites for steady-state conditions.

as described previously (25, 33). The suprabasal mitochondrial oxidative ATP synthesis rate was calculated from the immediate end-of-exercise rates of PCr resynthesis (V$_{ATP}$), which were calculated as V$_{ATP}$ = k$_{PCr}$·[PCr$_{depleted}$], where [PCr$_{depleted}$] was determined as the difference between resting and exercising [PCr] from the fully relaxed metabolite spectra.

^{31}P MRS analysis. All spectra were analyzed in jMRUI software (23) and phased and fitted to Lorentzian line shapes using the AMARES (36) algorithm with prior knowledge relating to resonant frequencies, j-coupling patterns, and relative amplitudes. Unlike the resting measurements, no averaging took place during exercise acquisitions and the SAT and CONT individual spectra were fitted (Fig. 2), thereby allowing for any change in the P$_i$ chemical shift over time. IR spectra were averaged for each TI prior to fitting. The γ-ATP resonance from the corresponding resting or exercising metabolite spectra was used for calculation of metabolite concentrations, assuming an [ATP] of 8.2 mM (17). The intracellular pH was determined from the chemical shift of P$_i$ relative to PCr (1), and the free concentration of ADP was calculated using established methods (1)

assuming a total creatine pool of 42.5 mM (17). Due to the nonconventional line shapes of the phosphomonoester (PME) resonances, [PME] was determined by integration techniques. This involved using the averaged metabolite spectra and applying an optimized line broadening, equivalent to that of 0.75*(line width of one singlet of the γ-ATP resonance doublet) before integrating the PME (5.9–7.5 parts per million) and γ-ATP resonances using the cut-and-weigh method. The Levenberg-Marquardt fitting algorithm within MATLAB (Math-Works, Natick, MA) was used to determine the T$_1$′ of P$_i$ from a two-parameter monoexponential fit, where M$_o$ was fixed [from the SAT spectrum at rest and from M$_o$-for-IR (Fig. 1) when exercising]. The first-order rate constant (k′) was determined according to the equation of Forsen and Hoffman: k′ = [(M$_o$ − M$_z$)/M$_z$](1/T$_1$′) and the P$_i$→ATP flux (V$_{Pi-ATP}$) by multiplication of k′ by the concentration of cytosolic P$_i$. The exercising V$_{Pi-ATP}$ component above the canonical net rate of oxidative ATP synthesis (surplus V$_{Pi-ATP}$) was calculated as V$_{Pi-ATP}$ − V$_{ATP}$, where V$_{ATP}$ was taken as the immediate end-of-exercise PCr resynthesis rate. Because V$_{ATP}$ reflects the rate of suprabasal oxidative ATP synthesis, resting V$_{Pi-ATP}$ was taken as the equivalent resting surplus V$_{Pi-ATP}$ measure. The rate constant for postexercise PCr resynthesis, k$_{PCr}$, was taken as a measure of muscle mitochondrial capacity (15).

Statistical analysis. Statistical analysis was performed using IBM SPSS Statistics 21 software (IBM, Armonk, NY) with two-tailed significance set at $P < 0.05$. A paired-samples t-test was used to test for significant differences between resting and exercising conditions using one data pair per person. Spearman's correlation analysis was used to test for significant correlations because this required fewer assumptions that could be violated. Tests for significant correlations were performed using all data sets from *group A* and *group B* volunteers, and by averaging multiple scans from *group B* to give one data point per person. Quantitative data are expressed as means ± SE.
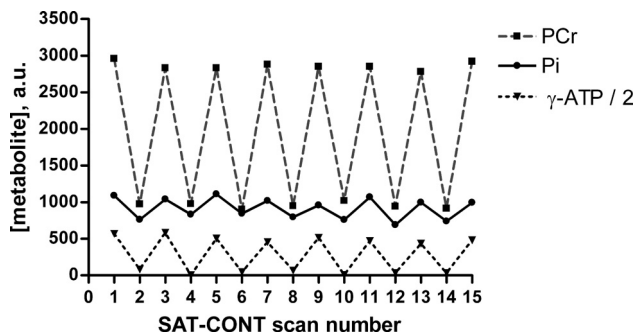

Fig. 2. Individual time course of metabolite concentrations obtained during steady-state exercise with alternating γ-ATP and control irradiation. Representative (*group B* volunteer) metabolite concentration time course of PCr (squares), P$_i$ (circles), and γ-ATP (triangles), obtained during steady-state exercise conditions with alternating frequency of saturation (SAT-CONT section in Fig. 1). Each x-axis point corresponds to a single spectrum. Even scan numbers correspond to spectra obtained with saturation of γ-ATP (SAT) and odd scan numbers to the equivalent control saturation frequency equidistant to P$_i$ (CONT). Consecutive points are joined by gray dashed (PCr), solid black (P$_i$), and dotted black (γ-ATP) lines to aid visualization.

RESULTS

All participants completed the exercise protocol and were fully compliant with the exercise instructions, resulting in no spectral exclusions. One scan (from a volunteer in *group B*) was lost due to broadband amplifier hardware failure and the ST data for another scan (of a volunteer in *group A*) were lost due to an incorrect saturation frequency. One partici-
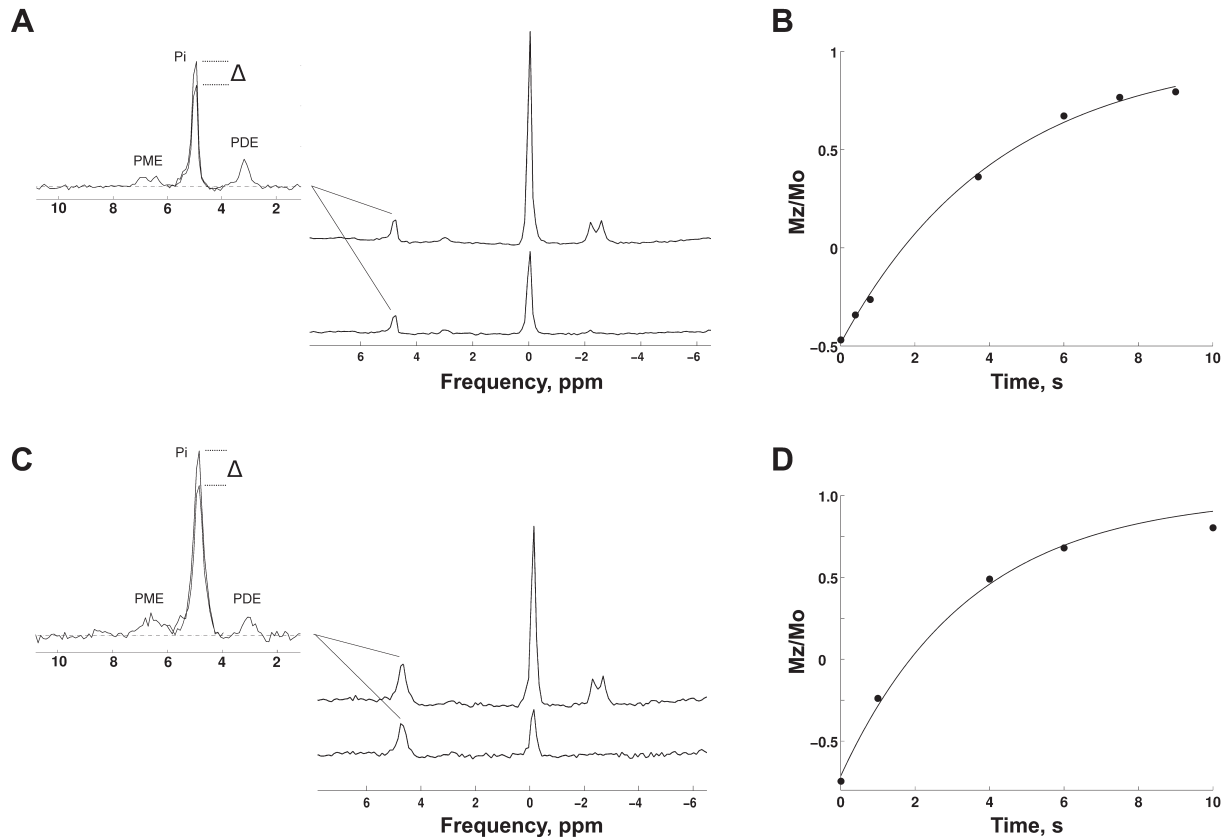
Fig. 3. ^{31}P MRS measurements of P$_i$→ATP flux at rest and during steady-state exercise. Representative saturation transfer (ST) spectra at rest (*A*) and during steady-state exercise (*C*), with saturation of the γ-ATP resonance (SAT) (*A* and *C, lower right*) and corresponding control spectrum (CONT) (*A* and *C, upper right*). The CONT spectra show the phosphomonoester (PME), P$_i$, and phosphodiester (PDE) resonances (*A* and *C, left*), superimposed with the SAT P$_i$ resonance to show the difference (Δ) in P$_i$ resonance. Corresponding inversion recovery plot for measurement of the P$_i$ T$_1$ in the presence of γ-ATP saturation both at rest (*B*) and during steady-state exercise (*D*).

pant in *group B* declined to provide a resting ST measure during the final visit but completed the exercise protocol, and another participant (in *group A*) failed to reach the steady-state exercise conditions, and that volunteer's ST exercise data were excluded. All remaining data were used.

Figure 2 illustrates the consistency of the steady-state exercise conditions and the changes in metabolite signals during saturation of the γ-ATP resonance in a representative individual.

Figure 3 shows typical saturation transfer spectra and inversion recovery plots obtained at rest and during steady-state exercise.

Table 1 shows mean rest and exercise values of key ^{31}P MRS measures. The overall mean fractional PCr depletion at steady-state exercise was $25 \pm 3\%$ ($n = 20$), and the mean postexercise PCr recovery rate constant (k$_{PCr}$) was 1.86 ± 0.16 min^{-1} ($n = 11$, one k$_{PCr}$ value per person). The mean change in pH$_i$ at the end of exercise bout 1, compared with resting conditions, was -0.051 ± 0.016 ($n = 20$). Splitting of the P$_i$

Table 1. *Mean resting and exercising ST and PCr resynthesis measures*

	Resting	Exercising	Paired-Samples Difference*	*P*†
ST, $n = 9$				
[P$_i$], mM	3.37 ± 0.18	10.23 ± 1.10	6.9 ± 1.1	<0.001
T$_1'$, s	4.5 ± 0.1	4.8 ± 0.3	0.3 ± 0.3	0.376
k′, min^{-1}	2.98 ± 0.35	2.44 ± 0.16	-0.54 ± 0.39	0.204
V$_{Pi-ATP}$, mM/min	9.8 ± 0.9	25.0 ± 2.9	15.1 ± 3.5	0.003
PCr resynthesis, $n = 11$				
[PCr], mM	32.9 ± 1.0	23.5 ± 1.2	-9.3 ± 1.2	<0.001
V$_{ATP}$, mM/min	‡	16.5 ± 1.8		ND

ST, saturation transfer; P$_i$, inorganic phosphate; T$_1'$, apparent longitudinal relaxation time of P$_i$ in the presence of saturation of the γ-ATP resonance; k′, first-order rate constant; V$_{Pi-ATP}$, rate of P$_i$→ATP flux; [PCr], concentration of phosphocreatine; V$_{ATP}$, suprabasal oxidative rate of ATP synthesis determined from immediate end of exercise PCr resynthesis; ND, not determined. Values are means $\pm$ SE. Data from volunteers in *group B* were averaged to provide one value per person to avoid inappropriate weighting. *Paired-samples difference (exercising-resting). †Paired-samples *t*-test to test for significant differences between rest and exercising conditions. ‡For comparison with exercising, this is 0.0 because V$_{ATP}$ reflects suprabasal oxidative ATP synthesis. The net rate of basal oxidative ATP turnover is thought to be approximately 0.5 mM/min (16).

peak occurred only in one individual in *group A*, who also had the lowest exercise pH$_i$ and the highest exercising V$_{Pi\text{-}ATP}$ of 39 mM/min, and in this individual the two P$_i$ resonances were fitted and then summed.

Resting V$_{Pi\text{-}ATP}$ did not correlate significantly with resting [P$_i$], [ADP], or [H$^+$] (all $P > 0.2$, $n = 18$, or $P > 0.5$, $n = 10$ averaging multiple scans from *group B*).

Figure 4 compares V$_{Pi\text{-}ATP}$ during exercise with the immediate end-of-exercise rate of suprabasal oxidative ATP synthesis, measured as the initial PCr recovery rate (V$_{ATP}$). Figure 4*A* shows the relationship between the two, with the line of identity for comparison; Figure 4*B* replaces the absolute V$_{Pi\text{-}ATP}$ flux with the increment in V$_{Pi\text{-}ATP}$ above the resting value. V$_{ATP}$ correlated significantly with both the exercising V$_{Pi\text{-}ATP}$ ($r = 0.552$, $P = 0.017$, $n = 18$) (Fig. 4*A*) and the suprabasal increment in V$_{Pi\text{-}ATP}$ ($r = 0.500$, $P = 0.041$, $n = 17$) (Fig. 4*B*), but this fell outside statistical significance when averaging the multiple scans in *group B* ($r = 0.65$, $P = 0.058$ and $r = 0.567$, $P = 0.112$, respectively, $n = 9$). It is clear that surplus V$_{Pi\text{-}ATP}$ (i.e., V$_{Pi\text{-}ATP}$ − V$_{ATP}$, the vertical distance above the line of identity in Fig. 4*A*), does not, on average, change over this range. Using all data points, exercising surplus V$_{Pi\text{-}ATP}$ was not correlated with exercising [P$_i$], [ADP], or [H$^+$] (all $P > 0.4$, $n = 18$), but was correlated with exercising [P$_i$] when averaging the multiple scans in *group B* ($P = 0.02$, $n = 9$).
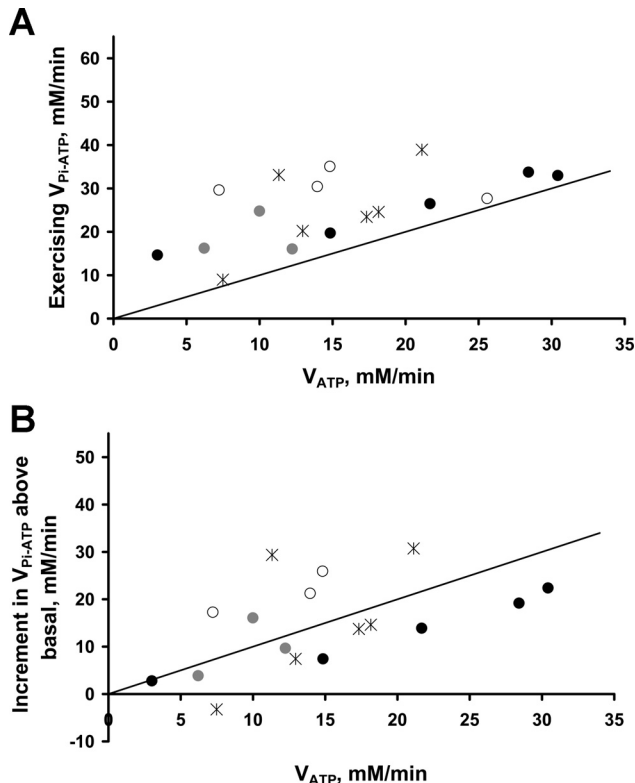
Fig. 5. Paired-samples difference (Δ) in surplus P$_i$→ATP flux and substrate concentrations of the enzymes GAPDH and phosphoglycerate kinase (PGK) between steady-state exercise and resting conditions. Paired-samples ($n = 9$) mean difference ± SE (exercising-resting values) for surplus V$_{Pi\text{-}ATP}$ and substrate concentrations of the enzymes GAPDH and PGK: P$_i$, ADP, and H$^+$. Surplus V$_{Pi\text{-}ATP}$ was calculated by subtracting the net rate of oxidative ATP synthesis, V$_{ATP}$ (estimated as the immediate postexercise PCr resynthesis rate), from the rate of P$_i$→ATP flux during exercise (V$_{Pi\text{-}ATP}$) to provide an estimate of the component of the ST measurement not explained by suprabasal mitochondrial ATP synthesis. Data from volunteers in *group B* have been averaged to provide one value per person to avoid inappropriate weighting (hence $n = 9$). A paired-samples *t*-test was used to test for significant differences between resting and exercising conditions (*P* values shown).

Figure 5 shows this work rate-invariance for surplus V$_{Pi\text{-}ATP}$ as the lack of a significant difference ($P = 0.912$, $n = 9$) between resting and exercising surplus V$_{Pi\text{-}ATP}$, as assessed by a paired-samples *t*-test.

Figure 6 examines the relationship between V$_{Pi\text{-}ATP}$ and concentration of PMEs. First, resting V$_{Pi\text{-}ATP}$ and resting [PME] were highly correlated ($r = 0.740$, $P < 0.001$, $n = 18$) (Fig. 6*A*), and also when averaging the multiple scans in *group B* ($r = 0.770$, $P = 0.009$, $n = 10$); these correlations remained significant after elimination of a possible outlier at low values. Second, exercising V$_{Pi\text{-}ATP}$ and exercising [PME] were also highly correlated ($r = 0.730$, $P = 0.001$, $n = 18$) (Fig. 6*B*) (or $r = 0.867$, $P = 0.002$, $n = 9$ when averaging the multiple scans in *group B*). V$_{Pi\text{-}ATP}$ comprises two components: a component due to net oxidative ATP synthesis (V$_{ATP}$), and a surplus. This correlation of V$_{Pi\text{-}ATP}$ during exercise with [PME] appears more closely related to the surplus exercising V$_{Pi\text{-}ATP}$ ($r = 0.534$, $P = 0.023$, $n = 18$; or $r = 0.65$, $P = 0.058$, $n = 9$) (Fig. 6*C*, gray and black symbols) than the V$_{ATP}$ ($r = 0.261$, $P = 0.295$, $n = 18$; or $r = 0.067$, $P = 0.865$, $n = 9$) contribution to exercising V$_{Pi\text{-}ATP}$. Linear regression using both resting and exercising data ($n = 36$) found [PME] to be a significant predictor of surplus V$_{Pi\text{-}ATP}$ ($R^2 = 0.291$, $P = 0.001$). Supplementing [PME] with other measured variables revealed that V$_{ATP}$, [P$_i$], and [ADP] were also significant predictors of surplus V$_{Pi\text{-}ATP}$, the models yielding the following results: [PME] and V$_{ATP}$ ($R^2 = 0.572$, [PME] and V$_{ATP}$ both $P < 0.001$); [PME] and [P$_i$] ($R^2 = 0.467$, [PME] $P < 0.001$, [P$_i$] $P = 0.002$); and [PME] and [ADP] ($R^2 = 0.369$, [PME] $P < 0.001$, [ADP] $P = 0.051$). In these models V$_{ATP}$, [P$_i$], and [ADP] were all significant negative predictors of surplus V$_{Pi\text{-}ATP}$ and hence had a significant effect in reducing the surplus V$_{Pi\text{-}ATP}$. This can be seen in Figure 6*C*, where for a given [PME] the surplus V$_{Pi\text{-}ATP}$ appears lower when exercising at high V$_{ATP}$. The [PME] and V$_{ATP}$ model yielded the highest correlation coefficient, and predicted a surplus V$_{Pi\text{-}ATP}$ = 4.681 + 5.096 [PME] − 0.335 V$_{ATP}$. When averaging the multiple scans in *group B* ($n = 19$),

Fig. 4. Steady-state rates of exercising P$_i$→ATP flux and its increment above basal levels, compared with measures of oxidative ATP synthesis rates. Exercising steady-state rates of P$_i$→ATP flux (V$_{Pi\text{-}ATP}$) (*A*) and its increment above basal levels (*B*), plotted against oxidative ATP synthesis rates (V$_{ATP}$) as measured from the immediate end-of-exercise PCr resynthesis rate. Black stars represent individuals in *group A*, and multiple scans of the three volunteers in *group B* are denoted by circles of black, gray, and white, respectively. The solid line represents unity equivalence of the two rates.
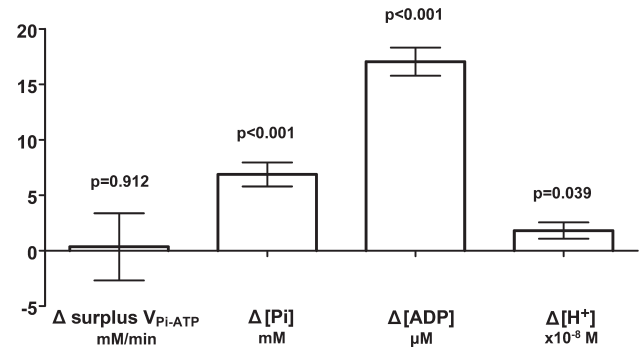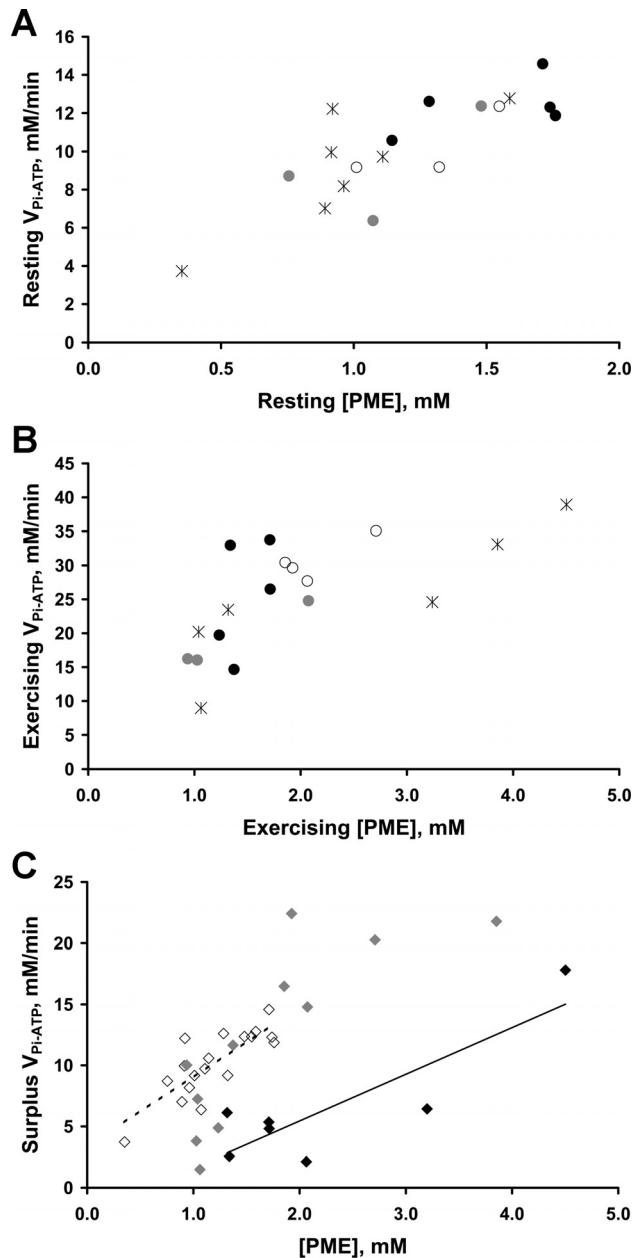
Fig. 6. Relationship of the P$_i$→ATP flux with the concentration of phosphomonoester (PME), at rest and during steady-state exercise. A: correlation of resting P$_i$→ATP flux (V$_{Pi-ATP}$) with resting [PME] ($r = 0.740$, $P < 0.001$, $n = 18$). B: relationship of exercising V$_{Pi-ATP}$ with exercising [PME] ($r = 0.730$, $P = 0.001$, $n = 18$). As in Fig. 4, black stars represent the individuals in *group A*, and the multiple scans of the three volunteers in *group B* are denoted by circles of black, gray, and white, respectively. C: surplus V$_{Pi-ATP}$ relative to [PME] at rest (white diamonds, $n = 18$) and during exercise (gray and black diamonds, $n = 18$). Surplus V$_{Pi-ATP}$ was calculated by subtracting the rate of suprabasal oxidative ATP synthesis, V$_{ATP}$ (estimated as the immediate postexercise PCr resynthesis rate), from the exercising V$_{Pi-ATP}$. Resting V$_{Pi-ATP}$ alone was used for the equivalent measure in resting muscle, where suprabasal ATP synthesis is by definition zero. Linear regression using both resting and exercising data ($n = 36$) found that in addition to [PME], V$_{ATP}$ was also a significant negative predictor of surplus V$_{Pi-ATP}$ (both [PME] and V$_{ATP}$ $P < 0.001$). This is illustrated schematically here by dividing the exercising data into low (0.0–14.9 mM/min) and high (15.0–30.5 mM/min) exercising V$_{ATP}$ groups denoted by gray and black diamonds, respectively. To aid visualization the dashed and solid black lines represent the trend lines for resting and high-exercising V$_{ATP}$ groups, respectively, and highlight the association of V$_{ATP}$ with reductions in surplus V$_{Pi-ATP}$ for a given [PME].

only [PME] alone ($R^2 = 0.675$, [PME] $P = 0.002$) and [PME] with V$_{ATP}$ were significant predictors ($R^2 = 0.787$, [PME] $P < 0.001$ and V$_{ATP}$, $P = 0.02$). Figure 6C also illustrates the apparent work-rate invariance of surplus V$_{Pi-ATP}$ between resting and exercising conditions (as in Fig. 5), and suggests how this may be the result of the counteracting effects of increasing [PME] and decreasing V$_{ATP}$ on the surplus V$_{Pi-ATP}$. These relationships appear to underpin some of the variation in Figure 4.

Age correlated significantly with k$_{PCr}$ ($r = -0.679$, $P = 0.022$, $n = 11$), but not with resting V$_{Pi-ATP}$ ($P = 0.44$). Resting V$_{Pi-ATP}$ did not correlate with k$_{PCr}$ ($P = 0.347$). Also, k$_{PCr}$ was not significantly correlated with exercising V$_{Pi-ATP}$, its suprabasal increment, or the surplus exercise V$_{Pi-ATP}$.

DISCUSSION

The novel exercise protocol shown in Figure 1 has allowed ST measurements of steady-state P$_i$→ATP flux over a range of workloads in human skeletal muscle with limited acidification. Minimizing acidification is important for two reasons. First, the relationships among pH, [PCr], and [ADP] imposed by the creatine kinase equilibrium mean that the interpretation of postexercise PCr recovery kinetics in terms of mitochondrial function is more straightforward. Specifically, a low pH is associated with slower PCr recovery for reasons that have nothing to do with any change in underlying mitochondrial function (15). Second, the use of a nonacidifying exercise protocol limits the contribution of net glycolytic ATP production to the measured P$_i$→ATP flux. From the known stoichiometry of aerobic glycolysis (4), a reasonable approximation for the aerobic glycolytic rate in C6 units is 1/30 of the rate of ATP synthesis. This is an upper limit because it assumes, unrealistically (28), zero contribution by oxidizing fat. In our experiments the rate of oxidative ATP synthesis is estimated as V$_{ATP}$, the initial postexercise rate of PCr resynthesis, and the highest measured value of V$_{ATP}$ (Fig. 4) implies, therefore, an aerobic glycolytic rate of only ~1 mM/min, or a net glycolytic ATP production rate of ~2 mM/min. Pyruvate can also be reduced to lactate instead of being oxidized, and the rate of this can be estimated from the change in pH (14, 18). The average pH decrease was ~0.05 units, which previous studies suggest would drive a H$^+$ efflux rate of ~0.4 mM/min (19). Consumption of H$^+$ in the creatine kinase reaction can be ignored because there was no change in steady-state [PCr]. Therefore, the anaerobic glycolytic ATP production rate is ~0.4 mM/min, representing a net glycolytic ATP production rate of no more than ~2.4 mM/min.

The surplus P$_i$→ATP flux remained approximately constant (Figs. 4 and 5) over the range from rest to the highest workloads undertaken (low to moderate respiration rates). This is consistent with inferences drawn from the stimulated rat hindlimb data (7, 11, 13). Similar invariance was also reported over low to moderate workloads in epinephrine-infused lamb myocardium; however, the fact that in that system P$_i$ and ADP concentrations do not vary with workload (26) complicates meaningful comparison. In partial contrast, in glucose-perfused rat myocardium over moderate to high workloads the surplus P$_i$→ATP flux appeared to decrease with increasing workload (20).

We also report for the first time the relationships between P$_i$→ATP flux and PME concentration (Fig. 6), which included significant correlations of the [PME] with resting, exercising, and surplus P$_i$→ATP flux. At rest and at the exercise intensities used in our study, the PME resonance is almost exclusively comprised of sugar phosphates (18), mainly glucose 6-phosphate (~80%) fructose 6-phosphate (~15%), and glucose 1-phosphate. The relationship of P$_i$→ATP flux with a [PME] that contains major contributions from glycolytic pathway substrates appears to be consistent with a large glycolytic P$_i$-ATP exchange contribution. GAPDH and PGK catalyze the coupled reaction: GAP + P$_i$ + NAD$^+$ + ADP ↔ NADH + H$^+$ + 3PG +ATP.

While there was little change in [H$^+$] there were substantial increases in [P$_i$] and [ADP] between rest and exercise, yet the overall surplus P$_i$→ATP flux remained unchanged (Fig. 5). One possible explanation for this is that the P$_i$↔ATP exchange catalyzed by GAPDH and PGK may be also dependent on the concentration of the downstream glycolytic intermediate, 3-phosphoglycerate, [3PG], which would be expected to follow, at least to some extent, the concentration of the sugar phosphates represented by the PME resonance. Experiments with isolated GAPDH and PGK have shown a dependence of the exchange on 3PG concentration (8), although the effects of this are difficult to deconvolve from changes in the equilibrium concentrations of the other substrates of the GAPDH/PGK couple; nevertheless, linear regression of the data shows [3PG] to be a significant predictor ($P < 0.001$). Another factor relevant to the relationship between P$_i$→ATP flux and [PME] might be the positive correlation of [PME] with [P$_i$] found when considering all data points (at rest $P = 0.038$; exercising $P = 0.012$, $n = 18$); however, (notwithstanding its purely algebraic contribution; V$_{Pi\text{-}ATP}$ = k′[P$_i$]), resting [P$_i$] was not significantly correlated with resting P$_i$→ATP flux, nor exercising [P$_i$] with exercising surplus P$_i$→ATP flux ($n = 18$).

In this work we have defined the response of V$_{Pi\text{-}ATP}$ in human skeletal muscle to large perturbations in the rate of ATP turnover, and partitioned it into the component due to net oxidative ATP synthesis, and what we have called surplus P$_i$→ATP flux. The approach taken does not of course allow us to experimentally dissect contributions to the latter, although we have shown that net glycolysis cannot be a significant contribution. However, the correlations and surprising lack of correlations we have observed between fluxes and concentrations allow some mechanistic speculation. Taking the resting and exercising data together, [PME] was a significant positive predictor of surplus P$_i$→ATP flux. Supplementing [PME], the suprabasal oxidative ATP synthesis rate was also found to be a significant predictor of the surplus flux, but acting in the opposite direction (Fig. 6C). The opposing effects of [PME] and V$_{ATP}$ resolve into the overall invariance in surplus P$_i$→ATP flux between resting and exercising conditions (Figs. 5 and 6C), and also explain some of the observed variation in P$_i$→ATP flux (Figs. 4 and 6). Because little is known about [3PG] levels in skeletal muscle during exercise, we can only speculate that this may reflect a lower 3PG:PME ratio at higher net glycolytic flux.

Reflecting on all potential routes for transfer of magnetization between P$_i$ and ATP, the P$_i$ and γ-ATP resonances can exchange magnetization in the coupled reactions catalyzed by GAPDH and PGK, and possibly also via the ATP synthase

(30), and via the unidirectional reactions of net ATP synthesis and breakdown. Net ATP synthesis, leading to direct transfer of magnetization between P$_i$ and ATP, takes place in the reaction catalyzed by mitochondrial ATP synthase and, indirectly, following net glycolytic flux through the GAPDH and PGK reactions, although we have shown the latter to be insignificant under the conditions of this study. Glycolytic ATP synthesis in the reaction catalyzed by pyruvate kinase will not result in transfer of magnetization between P$_i$ and γ-ATP. Net ATP breakdown, leading to direct transfer of magnetization between ATP and P$_i$, will take place in muscle predominantly in the reaction catalyzed by the myofibrillar ATPase. All other routes for exchange of magnetization between P$_i$ and the γ-phosphate resonance of ATP, most of which are less direct, are likely to be much slower.

In summary, we have demonstrated the feasibility of measuring P$_i$→ATP flux in human exercising muscle over varying workloads. The surplus P$_i$→ATP flux (that is, the amount by which it exceeds the known net mitochondrial ATP synthesis rate, estimated here from PCr recovery kinetics) is, on average, unchanged between rest and steady-state exercising conditions. This is in agreement with previous indirect inferences from rat skeletal muscle data, but seems surprising if (as commonly believed) the source of the surplus flux is P$_i$-ATP exchange mediated by the glycolytic enzymes GAPDH and PGK, in view of the substantial changes in [P$_i$] and [ADP] associated with increasing ATP turnover. However, some involvement of the GAPDH/PGK catalyzed exchange is suggested by the correlations observed between absolute and surplus P$_i$→ATP flux and [PME] both at rest and during exercise. We speculate that this may be due to downstream changes in [3PG] concentration, which has been shown to influence GAPDH/PGK exchange kinetics in vitro.

DISCLOSURES

No conflicts of interest, financial or otherwise, are declared by the authors.

AUTHOR CONTRIBUTIONS

A.S. and G.J.K. conception and design of research; A.S. and D.B.S. performed experiments; A.S. analyzed data; A.S., K.M.B., and G.J.K. interpreted results of experiments; A.S. prepared figures; A.S. and G.J.K. drafted manuscript; A.S., D.P., K.M.B., and G.J.K. edited and revised manuscript; A.S., D.B.S., G.B.W., D.P., T.A.C., K.M.B., and G.J.K. approved final version of manuscript.

REFERENCES

1. **Arnold DL, Matthews PM, Radda GK.** Metabolic recovery after exercise and the assessment of mitochondrial function in vivo in human skeletal muscle by means of ^{31}P NMR. *Magn Reson Med* 1: 307–315, 1984.
2. **Balaban RS, Koretsky AP.** *Interpretation of ^{31}P NMR saturation transfer experiments: what you can't see might confuse you.* Focus on "Standard

magnetic resonance-based measurements of the P$_i$→ATP rate do not index the rate of oxidative phosphorylation in cardiac and skeletal muscles". *Am J Physiol Cell Physiol* 301: C12–C15, 2011.

3. **Befroy DE, Rothman DL, Petersen KF, Shulman GI.** ^{31}P-magnetization transfer magnetic resonance spectroscopy measurements of in vivo metabolism. *Diabetes* 61: 2669–2678, 2012.

4. **Brand MD.** The efficiency and plasticity of mitochondrial energy transduction. *Biochem Soc Trans* 33: 897–904, 2005.

5. **Brindle KM.** ^{31}P NMR magnetization-transfer measurements of flux between inorganic phosphate and adenosine 5′-triphosphate in yeast cells genetically modified to overproduce phosphoglycerate kinase. *Biochemistry* 27: 6187–6196, 1988.

6. **Brindle KM.** ^{31}P nuclear magnetic resonance saturation transfer measurements of flux between inorganic phosphate and ATP in yeast cells over producing phosphoglycerate kinase. *Biochem Soc Trans* 14: 1265, 1986.

7. **Brindle KM, Blackledge MJ, Challiss RA, Radda GK.** ^{31}P NMR magnetization-transfer measurements of ATP turnover during steady-state isometric muscle contraction in the rat hind limb in vivo. *Biochemistry* 28: 4887–4893, 1989.

8. **Brindle KM, Radda GK.** ^{31}P-NMR saturation transfer measurements of exchange between P$_i$ and ATP in the reactions catalysed by glyceraldehyde-3-phosphate dehydrogenase and phosphoglycerate kinase in vitro. *Biochim Biophys Acta* 928: 45–55, 1987.

9. **Campbell-Burk SL, Jones KA, Shulman RG.** ^{31}P NMR saturation-transfer measurements in *Saccharomyces cerevisiae*: characterization of phosphate exchange reactions by iodoacetate and antimycin A inhibition. *Biochemistry* 26: 7483–7492, 1987.

10. **Du F, Zhu XH, Zhang Y, Friedman M, Zhang NY, Ugurbil K, Chen W.** Tightly coupled brain activity and cerebral ATP metabolic rate. *Proc Natl Acad Sci USA* 105: 6409–6414, 2008.

11. **From AH, Ugurbil K.** Standard magnetic resonance-based measurements of the P$_i$→ATP rate do not index the rate of oxidative phosphorylation in cardiac and skeletal muscles. *Am J Physiol Cell Physiol* 301: C1–C11, 2011.

12. **Kacerovsky M, Brehm A, Chmelik M, Schmid AI, Szendroedi J, Kacerovsky-Bielesz G, Nowotny P, Lettner A, Wolzt M, Jones JG, Roden M.** Impaired insulin stimulation of muscular ATP production in patients with type 1 diabetes. *J Intern Med* 269: 189–199, 2011.

13. **Kemp GJ.** The interpretation of abnormal ^{31}P magnetic resonance saturation transfer measurements of P$_i$/ATP exchange in insulin-resistant skeletal muscle. *Am J Physiol Endocrinol Metab* 294: E640–E642, author reply, E643–E644, 2008.

14. **Kemp GJ.** Muscle studies by ^{31}P MRS. *eMagRes* 4: 525–534, 2015.

15. **Kemp GJ, Ahmad RE, Nicolay K, Prompers JJ.** Quantification of skeletal muscle mitochondrial function by ^{31}P magnetic resonance spectroscopy techniques: a quantitative review. *Acta Physiol* 213: 107–144, 2015.

16. **Kemp GJ, Brindle KM.** What do magnetic resonance-based measurements of P$_i$→ATP flux tell us about skeletal muscle metabolism? *Diabetes* 61: 1927–1934, 2012.

17. **Kemp GJ, Meyerspeer M, Moser E.** Absolute quantification of phosphorus metabolite concentrations in human muscle in vivo by ^{31}P MRS: a quantitative review. *NMR Biomed* 20: 555–565, 2007.

18. **Kemp GJ, Roussel M, Bendahan D, Le Fur Y, Cozzone PJ.** Interrelations of ATP synthesis and proton handling in ischaemically exercising human forearm muscle studied by ^{31}P magnetic resonance spectroscopy. *J Physiol* 535: 901–928, 2001.

19. **Kemp GJ, Thompson CH, Taylor DJ, Radda GK.** Proton efflux in human skeletal muscle during recovery from exercise. *Eur J Appl Physiol Occup Physiol* 76: 462–471, 1997.

20. **Kingsley-Hickman PB, Sako EY, Mohanakrishnan P, Robitaille PM, From AH, Foker JE, Ugurbil K.** ^{31}P NMR studies of ATP synthesis and hydrolysis kinetics in the intact myocardium. *Biochemistry* 26: 7501–7510, 1987.

21. **LaNoue KF, Jeffries FM, Radda GK.** Kinetic control of mitochondrial ATP synthesis. *Biochemistry* 25: 7667–7675, 1986.

22. **Laurent D, Yerby B, Deacon R, Gao J.** Diet-induced modulation of mitochondrial activity in rat muscle. *Am J Physiol Endocrinol Metab* 293: E1169–E1177, 2007.

23. **Naressi A, Couturier C, Devos JM, Janssen M, Mangeat C, de Beer R, Graveron-Demilly D.** Java-based graphical user interface for the MRUI quantitation package. *MAGMA* 12: 141–152, 2001.

24. **Newcomer BR, Boska MD.** T$_1$ measurements of ^{31}P metabolites in resting and exercising human gastrocnemius/soleus muscle at 1.5 Tesla. *Magn Reson Med* 41: 486–494, 1999.

25. **Phillips AC, Sleigh A, McAllister CJ, Brage S, Carpenter TA, Kemp GJ, Holland AJ.** Defective mitochondrial function in vivo in skeletal muscle in adults with Down's syndrome: a ^{31}P-MRS study. *PLoS One* 8: e84031, 2013.

26. **Portman MA.** Measurement of unidirectional Pi→ATP flux in lamb myocardium in-vivo. *Biochim Biophys Acta* 1185: 221–227, 1994.

27. **Prompers JJ, Wessels B, Kemp GJ, Nicolay K.** Mitochondria: investigation of in vivo muscle mitochondrial function by ^{31}P magnetic resonance spectroscopy. *Int J Biochem Cell Biol* 50: 67–72, 2014.

28. **Romijn JA, Coyle EF, Sidossis LS, Gastaldelli A, Horowitz JF, Endert E, Wolfe RR.** Regulation of endogenous fat and carbohydrate metabolism in relation to exercise intensity and duration. *Am J Physiol Endocrinol Metab* 265: E380–E391, 1993.

29. **Schmid AI, Schrauwen-Hinderling VB, Andreas M, Wolzt M, Moser E, Roden M.** Comparison of measuring energy metabolism by different ^{31}P-magnetic resonance spectroscopy techniques in resting, ischemic, and exercising muscle. *Magn Reson Med* 67: 898–905, 2011.

30. **Sheldon JG, Williams SP, Fulton AM, Brindle KM.** ^{31}P NMR magnetization transfer study of the control of ATP turnover in Saccharomyces cerevisiae. *Proc Natl Acad Sci USA* 93: 6399–6404, 1996.

31. **Shonk CE, Boxer GE.** Enzyme patterns in human tissues. I. Methods for determination of glycolytic enzymes. *Cancer Res* 24: 709–721, 1964.

32. **Shonk CE, Boxer GE, Majima H, Koven BJ.** Enzyme patterns in human tissues. II. Glycolytic enzyme patterns in nonmalignant human tissues. *Cancer Res* 24: 722–731, 1964.

33. **Sleigh A, Raymond-Barker P, Thackray K, Porter D, Hatunic M, Vottero A, Burren C, Mitchell C, McIntyre M, Brage S, Carpenter TA, Murgatroyd PR, Brindle KM, Kemp GJ, O'Rahilly S, Semple RK, Savage DB.** Mitochondrial dysfunction in patients with primary congenital insulin resistance. *J Clin Invest* 121: 2457–2461, 2011.

34. **Tannus A, Garwood M.** Adiabatic pulses. *NMR Biomed* 10: 423–434, 1997.

35. **van den Broek NM, Ciapaite J, Nicolay K, Prompers JJ.** Comparison of in vivo postexercise phosphocreatine recovery and resting ATP synthesis flux for the assessment of skeletal muscle mitochondrial function. *Am J Physiol Cell Physiol* 299: C1136–C1143, 2010.

36. **Vanhamme L, van den Boogaart A, Van Huffel S.** Improved method for accurate and efficient quantification of MRS data with use of prior knowledge. *J Magn Reson* 129: 35–43, 1997.

37. **Yerby B, Deacon R, Beaulieu V, Liang J, Gao J, Laurent D.** Insulin-stimulated mitochondrial adenosine triphosphate synthesis is blunted in skeletal muscles of high-fat-fed rats. *Metabolism* 57: 1584–1590, 2008.